

Bioinspiration & Biomimetics



PAPER

Turning kinematics of the scyphomedusa *Aurelia aurita*

RECEIVED
1 September 2023

REVISED
21 November 2023

ACCEPTED FOR PUBLICATION
11 January 2024

PUBLISHED
23 January 2024

J H Costello^{1,3,*} , S P Colin^{2,3} , B J Gemmell⁴ , J O Dabiri⁵ and E A Kanso⁶ 

¹ Biology Department, Providence College, Providence, RI 02918, United States of America

² Marine Biology and Environmental Science, Roger Williams University, Bristol, RI 02809, United States of America

³ Whitman Center, Marine Biological Laboratory, Woods Hole, MA 02543, United States of America

⁴ Department of Integrative Biology, University of South Florida, Tampa, FL 33620, United States of America

⁵ Graduate Aerospace Laboratories and Mechanical Engineering, California Institute of Technology, Pasadena, CA 91125, United States of America

⁶ Department of Aerospace and Mechanical Engineering, University of Southern California, Los Angeles, CA 90089, United States of America

* Author to whom any correspondence should be addressed.

E-mail: costello@providence.edu

Keywords: jellyfish, maneuverability, body rotation, skid turn, propulsion

Abstract

Scyphomedusae are widespread in the oceans and their swimming has provided valuable insights into the hydrodynamics of animal propulsion. Most of this research has focused on symmetrical, linear swimming. However, in nature, medusae typically swim circuitous, nonlinear paths involving frequent turns. Here we describe swimming turns by the scyphomedusa *Aurelia aurita* during which asymmetric bell margin motions produce rotation around a linearly translating body center. These jellyfish ‘skid’ through turns and the degree of asynchrony between opposite bell margins is an approximate predictor of turn magnitude during a pulsation cycle. The underlying neuromechanical organization of bell contraction contributes substantially to asynchronous bell motions and inserts a stochastic rotational component into the directionality of scyphomedusan swimming. These mechanics are important for natural populations because asynchronous bell contraction patterns are common *in situ* and result in frequent turns by naturally swimming medusae.

1. Introduction

Scyphomedusae are members of an ancient animal clade [1–3] that has successfully colonized a wide array of marine environments [4] where these animals are often important community components [5, 6]. Their early evolutionary origins within the animal kingdom are reflected in the relatively basal body plans [7, 8]. This organizational simplicity, combined with their high propulsive efficiency, has favored scyphomedusae (often termed jellyfish) as models of basic propulsive principles [9, 10] as well targets for robotic design applications [11–13]. Most of this work has taken advantage of the radial symmetry of oblate medusan bells performing synchronous, symmetrical bell contractions during successive, regularly spaced bell pulsations. One consequence of this work has been a greatly expanded understanding of propulsion by medusae moving along straightforward, linear trajectories.

However, in natural settings, medusae often follow less ordered trajectories with highly variable directions. Importantly, their natural swimming patterns often differ from regular, symmetrical bell contractions and diverge from simple linear pathways. In contrast to linear trajectories, directional changes by these medusae—turns—involve asymmetric bell motions that produce irregular vortex formations [14] accompanied by unbalanced force production across the swimming bell surfaces. Differential force distributions result in torque application across the bell and body rotation during swimming. The velocity of bell turning is strongly related to bell kinematic changes. Perhaps non-intuitively, maximum torque is generated during the early stages of bell contraction but maximum turning velocity is reached during the late stages of contraction when the bell’s resistance to rotation—its moment of inertia—is diminished by shape alterations that reduce the bell diameter in the direction of rotation [15]. This means that the

outstretched configuration of a relaxed bell effectively acts as a brake on the rotation of a turn during early contraction and the change in bell shape during late contraction releases that braking resistance, thereby increasing the velocity of turning. For this reason, bell kinematics provide valuable insight into turning movements that determine maneuvering by medusae. Although basic components of medusan turning have been well explored [15, 16], fine control of turning maneuvers requires more detailed description of bell kinematics during turns. The application of basic neurological [16, 17] and hydrodynamic patterns [14, 15] is mediated through kinematic patterns that determine turn magnitude and duration. Hence, quantitative characterization of bell kinematic patterns is critical for emulating the rotational motions of medusae during turns. Here we quantify the kinematic patterns that determine the extent of rotational motions during turns by members of a cosmopolitan scyphomedusan genus, *Aurelia*, as a means to predict and emulate jellyfish turn magnitudes.

2. Methods

2.1. Turn kinematics *in situ*

Turning patterns of individual *Aurelia aurita* were collected from *in situ* video sequences of medusan field aggregations in Greenwich Cove, Rhode Island, USA) [18]. *In situ* video of medusan swimming was taken at 30 fps (Hi8). Video required that the diver maintain a fixed location and filming direction while resting on the substrate as medusae were carried past the recording diver [18].

2.2. Turn kinematics in the laboratory

Medusae of juvenile jellyfish (*A. aurita*, 2–6 cm) were obtained from the New England Aquarium and maintained at 25 °C in 20 l aquaria. Single, representative animals were recorded while freely swimming in a 30 × 10 × 25 cm glass vessel, using laser sheet illumination methods reported previously [9]. The laser sheet allowed determination of the planar orientation of the medusae and only sequences in which animals stayed centered in the light plane were used for kinematic measurements. Turn kinematics were recorded at 250 or 1000 fps (Photron Fastcam SA3). Individual turn sequences were selected in order to compare kinematics during turns of different magnitudes. These turn sequences started and ended with initiation of bell contraction during a pulsation cycle so that the full contraction and recovery of the bell were recorded for each turn sequence. The duration of a full cycle varied between medusae and was influenced by the bell diameter [19]. In order to compare these turns of different duration, each pulsation cycle of a turn sequence was divided into 15 evenly spaced intervals for kinematic measurements. This process was repeated for pulsations over a range of

turn magnitudes from 0° to 60°. Bell margin and centroid positions as well as angular orientation were measured at each stage within a pulsation cycle for all turn magnitudes. The collection of different turn magnitudes with similar kinematic sample regimes formed the basis for comparing kinematic patterns occurring across a range of medusan turns.

2.3. Measurement of bell kinematics

Turning kinematics of individual medusae were based on image sequences collected both *in situ* and in the laboratory. Video sequences were converted to still image sequences using Adobe Premier. Only medusae that swam perpendicularly to the viewing field of the recording camera were measured so that only a small subset of suitable targets occurred within a larger series of swimming medusae. Angular changes during swimming utilized alterations in the angle of a line connecting opposing bell margins measured at the beginning and end of a pulsation cycle. *In situ* video possessed extensive depth of field that precluded defined spatial length scale measurements. In contrast, the high spatial and temporal definition of laboratory images allowed measurement of alterations in bell morphology and position during a graded series of turns by a variety of individuals. These kinematic analyses utilized ImageJ software [20] to measure x, y coordinates of bell margins and centroids during turns.

Bell centroids were measured from cross sectional areas of medusan bells during turn sequences. The linearity of the centroid paths was measured as net to gross displacement ration (NGDR),

$$\text{NGDR} = \frac{\text{ND}}{\text{TD}}$$

where ND is the net displacement of the bell centroid, i.e. the shortest distance between the trajectory start and end points, and TD is the total traveled distance between successive points of the bell centroid during a turn sequence. NGDR ratios vary from 0 to 1, with a completely linear trajectory characterized by a value of 1.0.

Synchrony between movements of opposite bell margins was measured as the relative difference in contraction times of inside and outside bell margins during a pulsation cycle. The first margin to contract was termed the inside margin. This was followed by contraction of the opposite, or outside, margin. The absolute difference (seconds) between the movements of inside and outside margins was normalized by the time for full contraction of the bell (seconds),

$$\text{Contraction synchrony} = \frac{t_i - t_o}{T}$$

where t_i and t_o represent the times at which the inside and outside margins, respectively, moved toward

the bell centroid and T represents the total time duration of the pulsation cycle. Normalization by total pulsation cycle time was performed because bell diameter affects the duration of pulsation cycles [19]—larger medusae take longer to complete a pulsation cycle. Our approach placed differences in opposite bell margin timing within the framework of overall bell pulsation differences that accompany variations in bell diameter. Units of time cancel in numerator and denominator so these values are dimensionless. Completely synchronous bell contraction with identical values of t_i and t_o results in a value of 0. Because the total contraction duration rarely exceeded half the total pulsation cycle duration (T), values for even the least synchronous contraction times did not exceed 0.40.

Contraction symmetry between opposite bell margins was measured as the ratio of the absolute values of the outside and inside margin tip distances from the bell centroid at each stage of the bell pulsation cycle as:

$$\text{Contraction symmetry} = \frac{|p_o - c|}{|p_i - c|}$$

where p_i and p_o represent the positions of the inside and outside margins, respectively, relative to the bell centroid, c , at any time during the pulsation cycle. Units in the numerator and denominator cancel, making this a dimensionless index. For completely symmetrical bell movements, each margin was equidistant from the bell centroid and the ratio was 1.0. Asymmetrical bell motions generated varying distances of the margins from the centroid and these were reflected in the ratio of inside to outside margin distances throughout a pulsation cycle. The maximum difference during a cycle represented the greatest degree of bell asymmetry and varied from 1.02 to 1.61.

2.4. Particle image velocimetry (PIV)

We used methods following Colin *et al* [21] and Gemmell *et al* [9] to quantify the movement of fluids around swimming *A. aurita*. Fluid motions utilized 2D PIV by placing individuals into glass filming vessels in filtered seawater seeded with 10 μ diameter hollow glass beads. *A. aurita* were illuminated using a red laser sheet (680 nm wavelength) and recorded at 250 or 1000 frames per second using a Photron Fastcam 1024 PCI video camera that was placed perpendicular to the laser sheet. The velocity vectors of particles illuminated in the laser sheet were quantified from sequential images that were analyzed using a cross correlation algorithm (LaVision Software). Image pairs were analyzed with shifting overlapping interrogation windows of decreasing size (64 x 64 pixels, then 32 x 32 pixels).

3. Results

3.1. Turning occurs through bell rotation superimposed upon linear translation by the center of mass during each pulsation cycle

In contrast to the symmetrical, synchronous bell pulsations patterns characterizing medusae swimming along a straight-line trajectory, turning medusae followed a stereotypic pattern involving asynchronous, asymmetrical bell contractions. The medusa's center of mass, indicated by the centroid, followed a primarily linear trajectory during most pulsation cycles, regardless of bell orientation changes during a pulsation (figure 1). During straight swimming, bell contraction and relaxation occurred approximately synchronously along the full extent of the bell margin (figures 1(A)–(E)). However, examination with high speed video (1000 fps) revealed that true synchrony is very rarely achieved during bell pulsation. Instead, disparities in contraction timing and extent (figures 1(F)–(J)) are typical during swimming by *A. aurita*.

Disparities in pulsation timing (synchrony) and extent (symmetry) across the bell create bell rotation during both contraction and recovery phases of the pulsation cycle. Bell rotation first becomes evident on the side towards which the medusa will rotate, here termed the inside of the turn. Bell curvature is distinctly different on the inside margin compared to the opposite, or outside margin (figures 1(G) and 2). The initial motion of the inside bell margin often generates a short period of bell rotation in the opposite direction of the ultimate rotation occurring over the full bell pulsation. This opposite-sense rotation occurs at the earliest stage of bell contraction (figure 2; $t = 0.4$ s). However, as the outside margin subsequently contracts, rotation direction shifts and increases, reaching peak angular velocity at near maximum bell contraction as indicated by minimum bell fineness (figure 2, $t = 0.6$ s).

Although maximum bell rotation occurs during the contraction phase, rotation can continue at a lower rate throughout the recovery phase of pulsation (figures 2 and 3). The rate and extent of rotation during recovery phase are also influenced by the symmetry of bell margin kinematics during recovery. In more extensive turns, the inside margin may remain contracted longer and relax more slowly than the outside margin (figures 3(C)–(F)). This asymmetry during relaxation causes water refilling the bell to flow disproportionately into the subumbrellar cavity of the outside margin and lengthens the relative duration of the recovery period as well as increases the extent of rotation that occurs during recovery. Prolonged asynchronous recovery periods can also lead to lateral drifting of the bell (figure 4(A)).

The variations in bell kinematics during both contraction and recovery phases resulted in variable

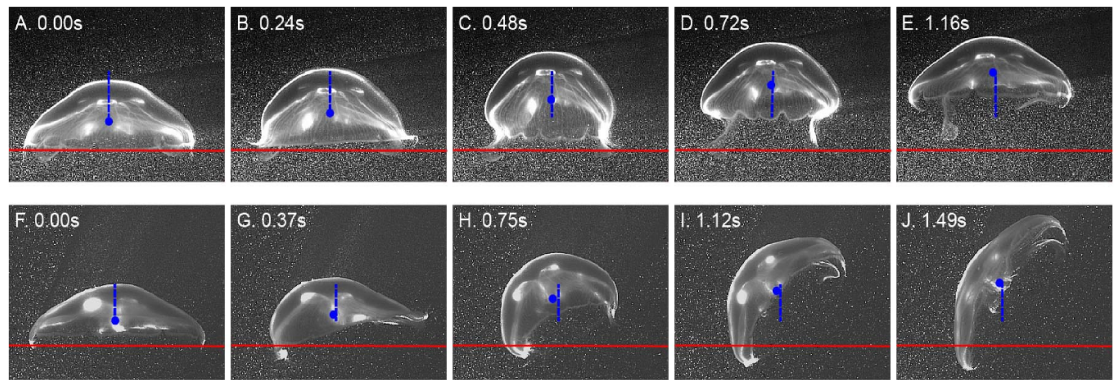


Figure 1. Bell translation and rotation during swimming by the scyphomedusa *Aurelia aurita*. (A)–(E) Straight trajectory swimming with relatively simultaneous and symmetrical pulsation cycle of a 5.2 cm diameter medusa. Blue circle denotes bell centroid position and blue line tracks centroid path during full pulsation cycle. Note the slight asymmetry in bell pulsation (B) and minor alteration in angular orientation between the start and end of pulsation. (F)–(J) Turning kinematics of a 6.2 cm diameter medusae illustrating the earlier movement (asynchrony) of the bell margin on the inside of the turn as it moves towards the bell's central axis, as well as the different curvature patterns (asymmetry) of bell contraction patterns of bell margins during the turn. Note that for both medusae, the centroid path is relatively linear.

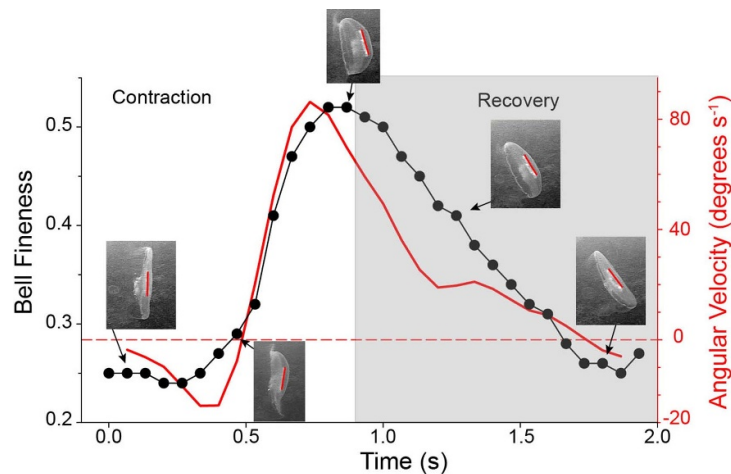


Figure 2. Relationship between bell deformation and angular velocity during a 39° turn by *Aurelia aurita* (~ 5.5 cm diameter). The upper surface of the gonads were in relief during the turn and served as a reference for body motion of this animal moving *in situ* (Greenwich Cove, RI, USA). Turns often involve an initial rotation counter to the final direction of the turn, indicated as a negative velocity, due to the curling deformation of the inside margin of the bell (second image from left). This changes as the outside margin contracts so that the greatest angular velocities, and most visible components of a turn, occur during the end of the contraction phase. Peak angular velocity slightly precedes peak bell fitness, as indicated by bell fitness. Note that turning can continue into the recovery phase even as angular velocity declines during that portion of the pulsation cycle. For this turn, 56% of total net angular change occurred during contraction and 44% during the recovery phase.

rotation around the bell center of mass—turning—as medusae swam. The pattern of differential margin movement around a linearly translating center of mass is generally consistent over a wide range of turn magnitudes by a variety of bell diameters (figures 5(A), (C), (E), (G), (I) and (K)). In all cases, the inside margin contracted towards the bell central axis first, followed by the outside margin sweeping inward towards the bell's central axis. Although this general pattern appears stereotypic, the specific phase relationship between inside and outside margin kinematics varied considerably between turns (figures 5(B), (D), (F), (H), (J) and (L)) and resulted in variation between the proportion of rotation

occurring during contraction and recovery phases (figure 6).

As a result of whole-body rotation during pulsation cycles, medusae move by saltatory swimming with shifting directions between pulses. Since the center of mass moves in a primarily linear trajectory, the orientation of the bell at the outset of a contraction sets the initial linear pathway for the center of mass trajectory during that pulsation cycle. Rotation during the pulsation determines the final bell orientation and sets the center of mass pathway for linear translation during the subsequent bell pulsation (figure 4). Since most pulsation cycles produce some rotation, these traits result in frequent

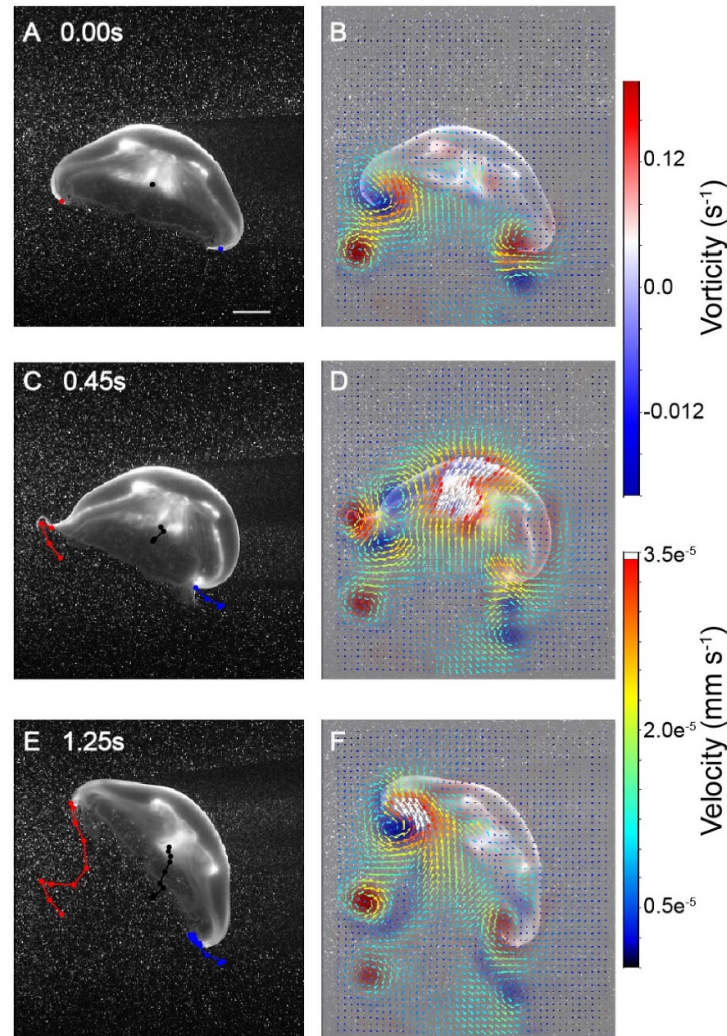


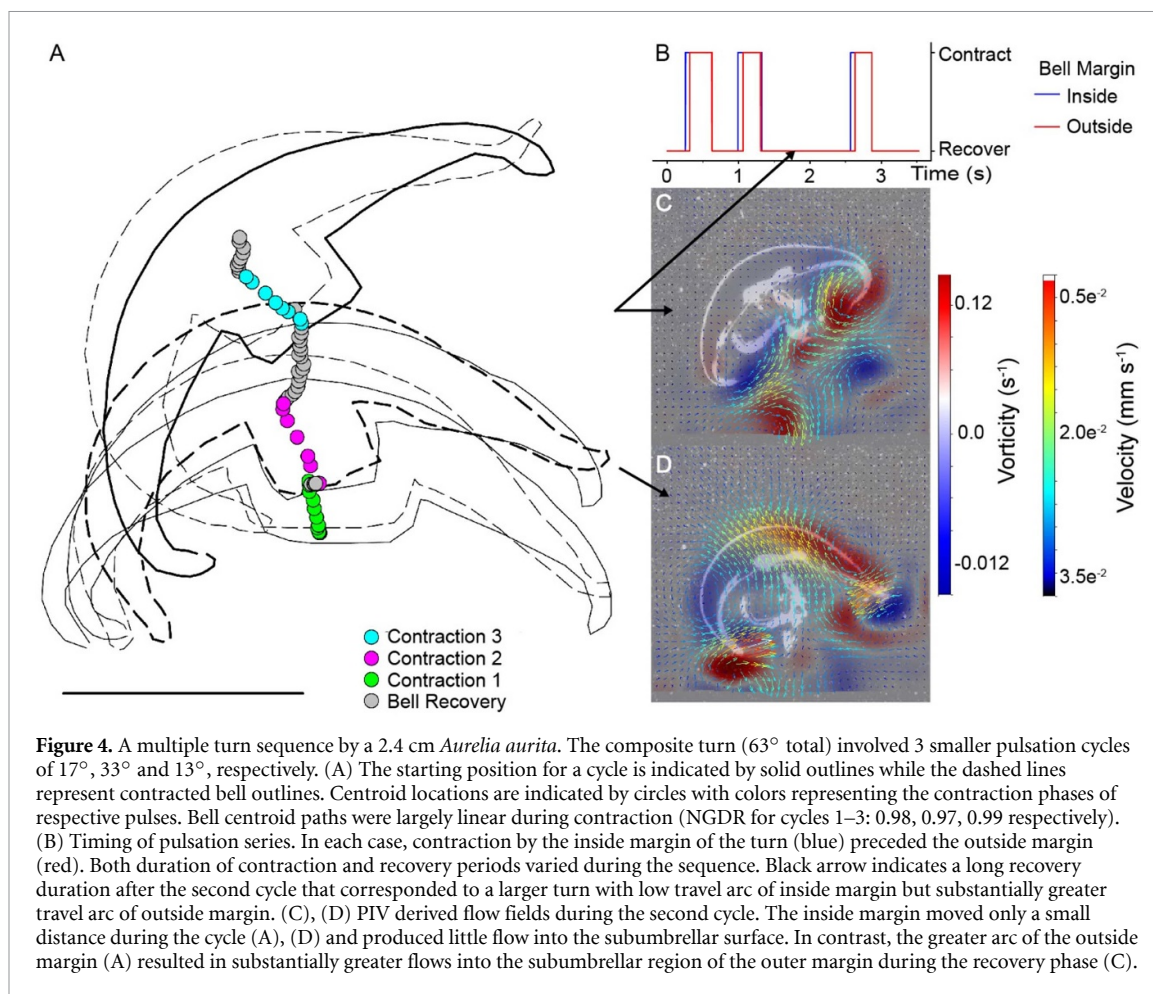
Figure 3. Fluid motions accompanying bell kinematics during a 30° turn by a 6 cm diameter *Aurelia aurita*. Bell motions and successive alterations (left panels (A), (C) and (E)) with corresponding fluid motions (right panels (B), (D) and (F)). Scale bar (panel A) represents 1 cm. Successive bell centroid (●), outside (●) and inside (●) bell margin locations are indicated in the left panels ((A), (C) and (E)). The turn begins as the inside margin moves towards the bell centroid while the outside margin moves outward and away from the centroid. Following contraction, the inside margin remains relatively stationary while the outside margin expands more rapidly and over a greater distance. The greater expansion of the outside margin is accompanied by the bulk of refilling flow entering the subumbrellar side of the outside margin. White vectors represent velocities exceeding the velocity scale. The bell centroid follows a relatively linear path as the bell rotates around it.

orientation changes—turns—by swimming *Aurelia* medusae.

3.2. Bell contraction synchronicity is a major predictor of rotation during bell pulsation cycles

Variations in bell kinematics—both synchrony and symmetry of bell margin motions—strongly influence the amount of bell rotation within a pulsation cycle. Because the contraction phase is the dominant contributor to overall rotation for most pulsation cycles (figure 6), contraction kinematics are strong predictors of total bell rotation during cyclic pulsation. The synchrony with which the margins of the bell contract is strongly related to the symmetry of bell movement on either side of a rotating bell

(figure 7(A)). Larger disparities in timing of contractions are significantly related to more extensive differences in curvature on the inside and outside of a turn. Although both asymmetry and asynchrony are strong indicators of overall turn magnitude, contraction synchrony provided the strongest correlation to overall turn magnitude (figures 7(B) and (C)). The reliability of contraction synchrony as an overall turn predictor is tempered by the fact that the recovery phase can also contribute to bell rotation (figure 2). Variations in bell margin kinematics during the recovery phase can be extensive (figure 4(B)), and those variations limit the extent to which contraction synchrony determines overall turn magnitude during a pulsation cycle (figures 5 and 7(C)).



4. Discussion

4.1. Translation and rotation during swimming by *Aurelia medusae*

Bell pulsation, particularly bell margin kinematics, generate hydrodynamic forces that propel the medusa forward (reviewed in [22]). Direct linear swimming relies upon the medusan bell contracting evenly across its entire surfaces so that force application is evenly distributed. The result of synchronous, symmetrical force application across the bell surface is linear translation of the body. Importantly, disparities in bell kinematics generate uneven forces along that bell that result in rotation during these bell pulsations [15, 16]. In addition to contraction, bell recovery kinematics that direct stopping vortices to ‘push’ the bell forward [9] also require symmetrical, synchronous bell relaxation in order to centrally position vortex flows that result in simple linear translation of the body through water. For these reasons, simple linear trajectories by swimming medusae require synchronous, symmetrical movements across the bell surface during both bell contraction and recovery phases of pulsation.

However, detailed measurements demonstrate that bell kinematics are rarely synchronous or

symmetrical for either contraction or recovery phases of a pulsation cycle [23]. Instead, a spectrum of variations in bell kinematics are associated with differing degrees of rotation as the bell center of mass translates forward during a pulsation cycle. Disparities in movement across the bell generate uneven forces across the bell surface which in turn generate uneven hydrodynamic forces across the bell and result in bell rotation [15]. Bell rotation is most often dominated by contraction kinematics and the best overall predictor of turn magnitude during a pulse is the degree of disparity, here termed the asynchrony, between the inside and outside margins of a turn during the contraction phase (figures 5 and 7(C)). These results agree with robotic evidence demonstrating that controlled turning has been achieved in jellyfish vehicles by varying the contraction synchrony of inside and outside margins [13, 24]. Swimming scyphomedusae demonstrate that additional rotation can be affected by asymmetrical bell kinematics during the recovery phase (figures 3–6), providing living scyphomedusae with rotational capabilities throughout the pulsation cycle. Interestingly, a number of more prolate species, including cubomedusae [25] often rotate substantially during the recovery portion of a pulsation cycle. Scyphomedusae such as *A. aurita* swim

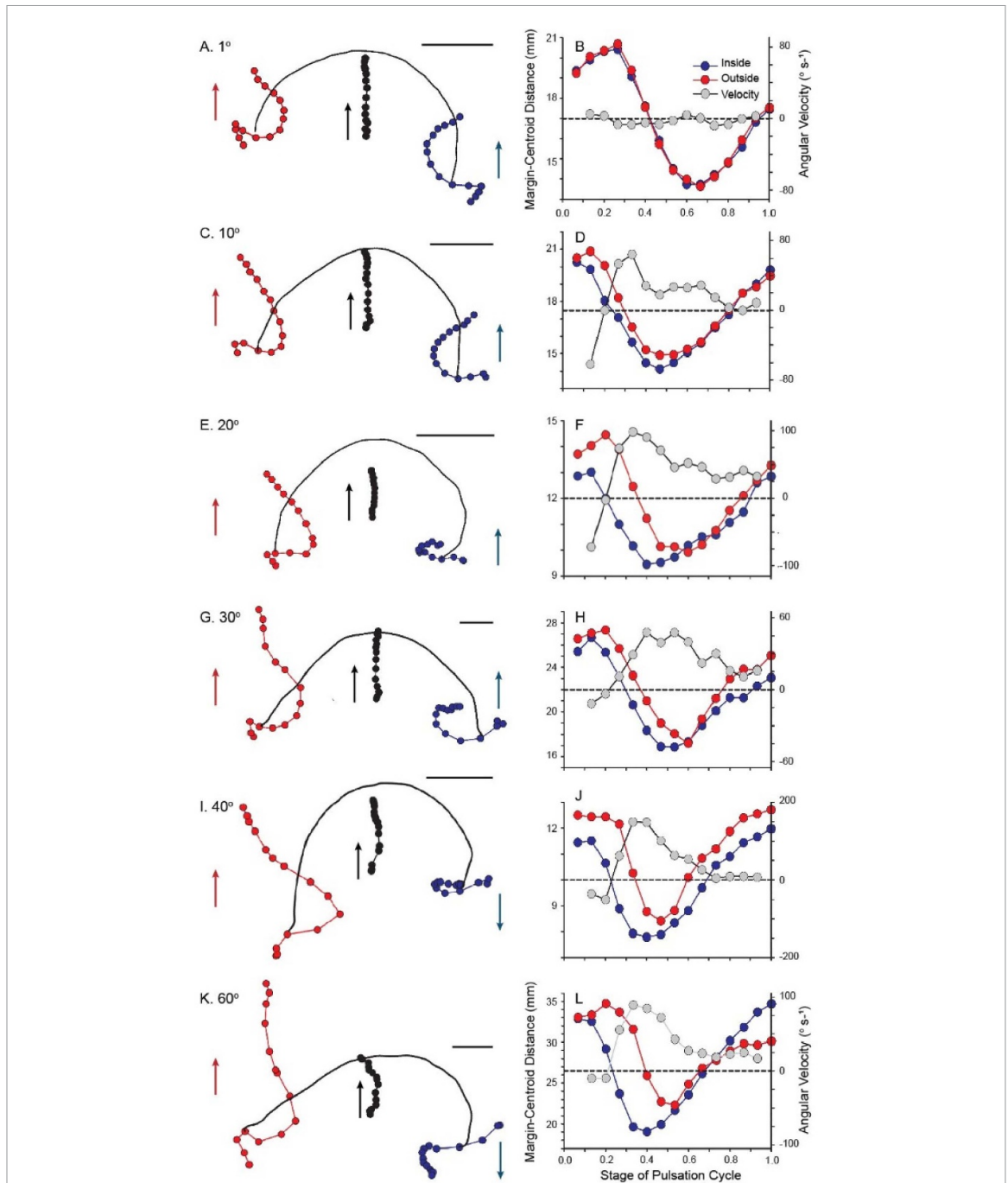
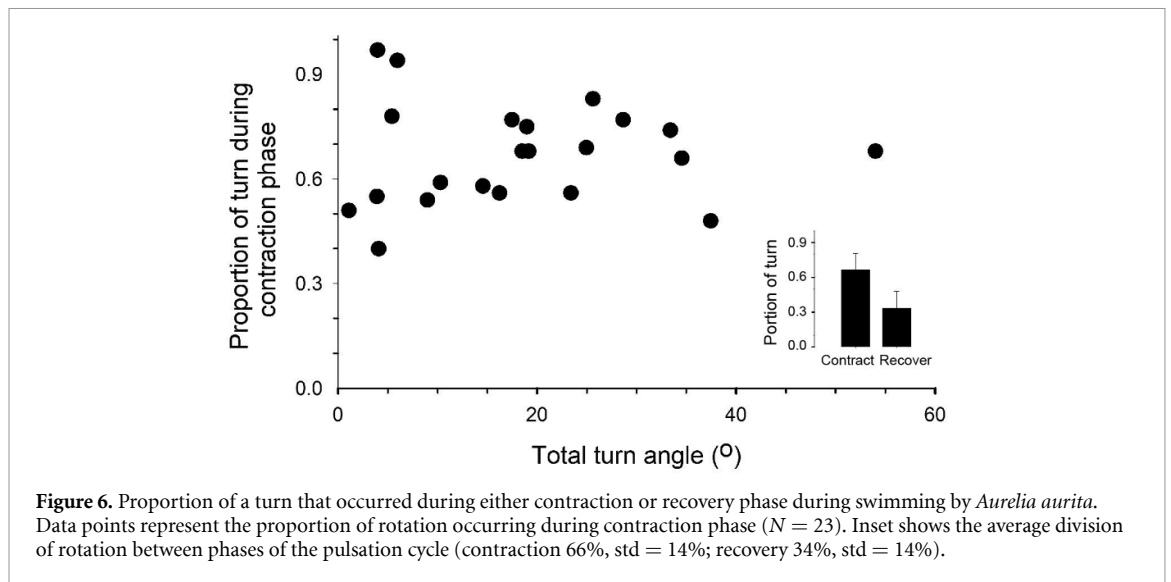


Figure 5. Kinematic patterns of bell motion through a graded range of turns by *Aurelia aurita*. Left column depicts a series of single-pulse turns from $\sim 1^\circ$ to 60° . Medusae were of variable diameter and black scale bars represent 1.0 cm for each of the sequences. Bell outlines illustrate the bell shape during the mid-contraction period of the pulsation cycle. As in figure 4, circles indicate successive positions of the bell centroid (black), inside (blue) and outside (red) margins. Arrows indicate the general direction of motion. The right column illustrates the position of the bell margins on the inside and outside of the turn relative to the bell centroid for each of the depicted turns. Grey circles represent angular velocity (degrees s^{-1}). Medusae were of different sizes and pulsation data were adjusted by the total duration of a pulse so that each cycle has a normalized time of 1.0. Bell centroids followed primarily linear paths and NGDR values for bell centroid paths were (A) 0.98, (C) 0.97, (E) 0.98, (G) 0.97, (I) 0.96, and (K) 0.92. For a minor turn (A), centroid motion translated along a linear path while the arc of both margins traveled similar distances and maintained similar positions relative to the centroid (B). Increasing turn angles were accompanied by greater disparity in bell margin motions relative to the centroid. The inside bell margin always initiated contraction before the outside margin began movement towards the bell centroid (B), (D), (F), (H), (J), (L). During more extreme turns of $>40^\circ$ (I)–(L), the inside and outside bell margins traveled in opposite directions relative to the centroid, demonstrating extensive bell rotation around the centroid as the medusa body translated forward during swimming.

nearly continuously [18] and variability in bell kinematics during these cyclic movements results in frequent changes in bell orientation—turns—between pulsations during swimming.

Although scyphomedusan turns are not rapid relative to other swimmers such as fish, the dynamics of their turns resemble mechanics of highly effective projectile turns. Linear continuation of the object's



center of mass while the surrounding body rotates are typical of ‘skid’ turns. The rapid alteration in directional heading possible via skid turns has led to adoption of this turning approach for a variety of missile control systems [26–28].

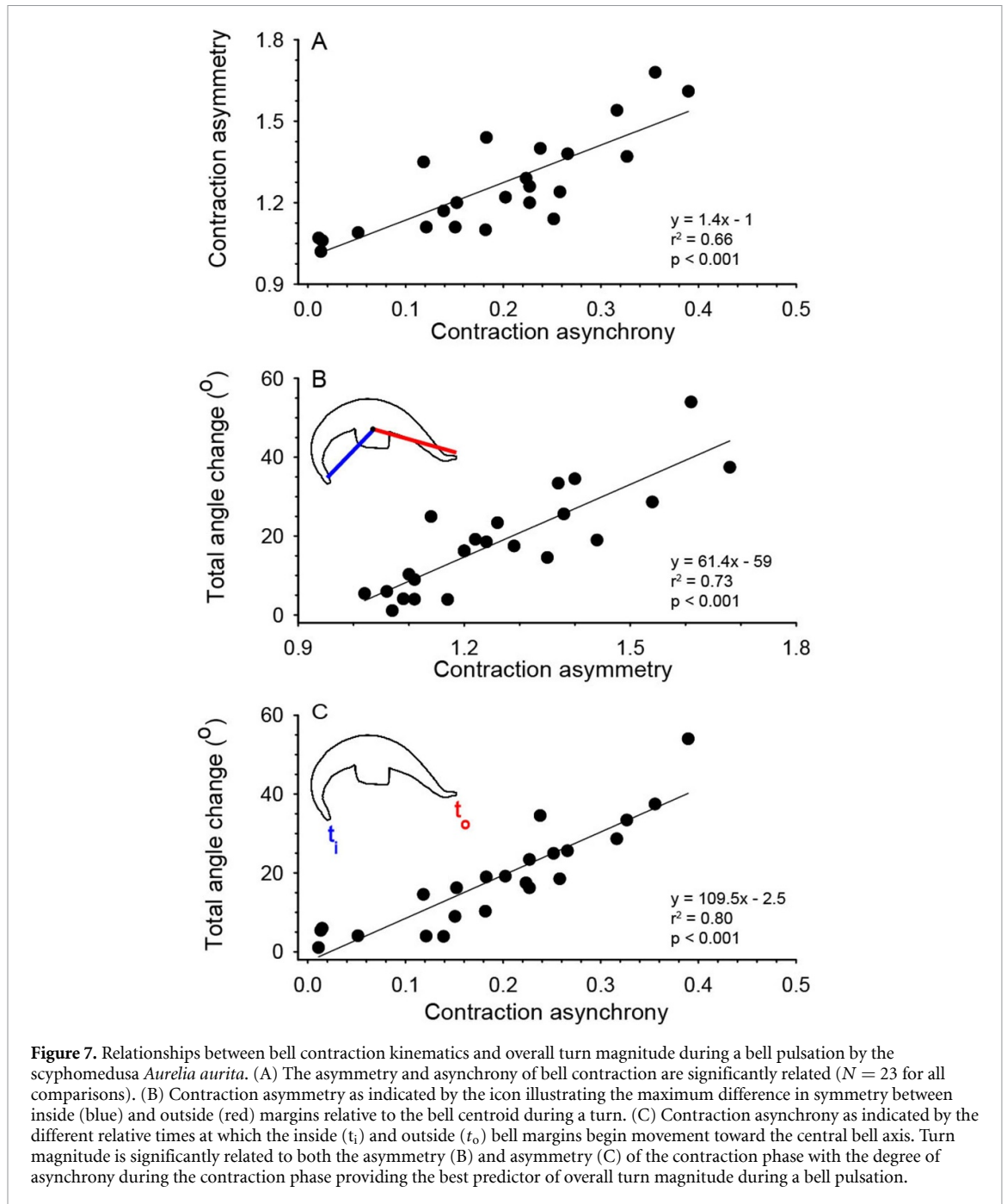
Frequent turning may be common among other species of scyphomedusae. Although we describe turning dynamics for *A. aurita*, fine-scale directional data from accelerometer tags on *Chrysaora fuscescens* indicate frequent turns that decline in magnitude exponentially [29] in a similar pattern to similarly to *A. aurita*. In contrast to the *Aurelia* field population that we studied, which demonstrated no consistent direction during their swimming, several studies of other *Aurelia* field populations describe oriented swimming [30–32]. Directional swimming may be adapted to local conditions [18, 33] and frequent turns may be cued to maintain a directed orientations as local conditions shift. Hence, frequent turns may help maintain directional swimming for a variety of local conditions.

4.2. Turning patterns reflect scyphomedusan neuromechanical organization

The neurological basis of scyphomedusan bell contraction has a long history of study that is well reviewed [34–36]. For scyphomedusae such as *Aurelia*, bell contraction is initiated by rhopalial pacemakers which generate action potentials that propagate non-decrementally [37, 38] across the bell through a bipolar nerve net. These action potentials stimulate subumbrellar circumferential myofibrils that contract, causing bell deformation. The primary nerve net system associated with these waves of neuromuscular activation is termed the motor nerve net (MNN). A second net of less clear function, appropriately termed the diffuse nerve net (DNN), also transmits action potentials through the bell. Transmission rates of the MNN are more rapid (45–50 cm s⁻¹ [37,

38]; compared to the slower DNN (0.2–2.0 cm s⁻¹ [39]; signals and the more rapid MNN is the primary driver of circular muscle contraction. However, the DNN may be involved with radial muscle contraction near the bell margin [14, 39, 40]. Each excitatory wave resets all other pacemakers and is followed by a refractory period for bell recovery. The eight rhopalial pacemakers of *Aurelia* alternate as sources for activation waves with each pacemaker exhibiting irregular activation frequencies [34]. The pacemaker with the fastest rhythm during a given interval drives the swimming rhythm until its frequency declines or a different pacemaker ascends to the controlling role [40]. A model of excitatory wave transmission indicates that variation of excitation transmission patterns can lead to asynchronous, asymmetric bell contraction [17]. Hoover *et al* [16] argue that, in addition to neurological wave propagation, mechanical wave propagation, dictated by material stiffness of the bell during contraction, influences the kinematics of bell contraction. Therefore, factors influencing bell stiffness, such as muscle tension and mesogleal fiber compression states, can influence the kinematic outcome of action potential wave transmission across the bell. Maximum contraction kinematics occur when bell material stiffness resonates at the same frequency as neurological wave transmission rates.

Neuromuscular control during bell recovery is less clearly documented than the contraction phase. Bell recovery involves termination of the contraction signal followed by a neural refractory period during which excitation waves do not propagate through the MNN. During this period, elastic energy stored within contractile fibers of the mesoglea cause bell shape to return to the uncontracted state and the bell expands to its maximum diameter. Since this period involves no MNN muscle excitation, synchronous, symmetrical bell recovery might be expected. However, as noted earlier by Horridge



(1956) and evident in measured bell kinematics (figures 3–5), bell recovery is often not symmetrical and this can lead to increased rotation during the recovery phase. Radial muscle contraction influenced by the DNN [14, 17, 39] is believed to strongly influence the margin kinematics during a turn and complex neuromuscular patterns during the recovery phase may involve DNN enervation during the MNN refractory period. However, the interactions of this doubly-enervated muscular system [34, 39] remain only partially documented.

These foundations of scyphozoan neuromuscular control are important for understanding the degree of stochastic variability that is largely inevitable within

both phases of cyclic bell pulsations. For example, completely synchronous contraction across the full bell surface is rare. This likely reflects the comparatively slow rates of neural wave transmission through the scyphozoan bipolar nerve nets. A MNN activation wave speed of 45 cm s^{-1} [37] across a 5 cm diameter bell results in a $\sim 0.1 \text{ s}$ delay between signal onset for one side of the bell relative to its arrival at the opposite bell margin. Pulse cycle duration of a 5 cm diameter *Aurelia* at 20° is approximately 1.2 Hz (figures 1(A)–(E)) and, based on the relationship between asynchronicity and turn magnitude (figure 7(C)), this would result in an approximately 7° turn due simply to scyphozoan neuromuscular

design. The timing and extent of bell contraction may be further modulated by variable mechanical wave transmission through bell materials [16, 41] that can either damp or accentuate contraction variations along the bell margins.

Variations in bell kinematics are not limited to the contraction phase but affect the recovery phase of bell pulsation. Medusae show considerable variation in bell relaxation rates for margins on either side of the bell during recovery phase (figure 4, see also [39, 42]). In some cases, the inside margin appears to remain partially contracted while the outside margin relaxes and expands. The DNN may act either independently or modulate MNN activity [17, 34, 39] to influence radial muscles and relaxation of the bell margin. Interactions involving DNN modulation of bell kinematics are less clearly understood than those of the MNN and add a level of complexity to the overall process of scyphozoan bell pulsation.

The inherent variability in neural and mechanical wave propagation has important consequences for overall medusan swimming. Variable bell kinematics cause variable torque applications [15, 16] that, in turn, cause bell rotation and turning during swimming. Turning can help maintain course heading during directed swimming [31, 43–46], but can also occur in the absence of distinct population-level directional swimming.

4.3. Inherent instability results in observed natural swimming patterns

The scyphozoan neuromuscular system embeds rotational instability within pulsed swimming by *A. aurita*. Although its bluff shape imparts passive stability to the medusan center of mass (figures 1 and 5), unpredictable alternations between control pace-makers, variable neural and mechanical wave rates and complex interactions between two major nerve nets (MNN and DNN) produce fluctuating rotational components within and between cyclic bell pulsations. Most pulsation cycles show some variability [23] and contribute to rotational variation during sequential bell pulsations.

A. aurita swimming exemplifies the integration of comparatively low performance, high variability components into an extremely successful organism. Their muscles are rudimentary [6] and their neural performance is highly variable without organization from a centralized brain [34]. That inherent neural variability, coupled with overall slow response times, precludes the impressively synchronized cohesion of more recently evolved groups such as fish [47] and krill [48] schools. Yet scyphozoan swimming is very effective for energy acquisition through predation [22] and is competent for population level responses to stimuli such as light [33] and currents [43]. Their limited swimming capabilities have not prevented ecological success. Instead, their swimming reflects effective integration of constrained neural

and mechanical components into a strategy that has enabled their roles as important planktonic predators. Understanding rotational mechanics of naturally occurring medusae also provides a pathway for maintaining jellyfish vehicle stability in the face of perturbation occurring under a variety of naturally occurring conditions.

Data availability statements

All data that support the findings of this study are included within the article (and any supplementary files). Data will be available from 01 January 2026.

Acknowledgment

We wish to thank the New England Aquarium (Protocol 2022-14 to JHC) for generously providing *Aurelia aurita* medusae for laboratory work.

Conflict of interest

The authors declare no competing interests.


Funding

We gratefully acknowledge the US NSF (CBET-2100705, IOS-2114171 to JHC, CBET-2100156, IOS-2114169 to SPC, CBET-2100703 to BJG, CBET-210020, RAISE IOS-2034043 to EK) and the US ONR (N00014-23-1-2754 to JHC, N00014-22-1-2655, N00014-19-1-2035, N00014-19-1-2035 to EK).

ORCID iDs

J H Costello  <https://orcid.org/0000-0002-6967-3145>

S P Colin  <https://orcid.org/0000-0003-4463-5588>

B J Gemmell  <https://orcid.org/0000-0001-9031-6591>

E A Kansa  <https://orcid.org/0000-0003-0336-585X>

References

- [1] McCarthy C G, Mulhair P O, Siu-Ting K, Creevey C J and O'Connell M J 2023 Improving orthologous signal and model fit in datasets addressing the root of the animal phylogeny *Mol. Biol. Evol.* **40** msac276
- [2] Dunn C W, Giribet G, Edgecombe G D and Hejnol A 2014 Animal phylogeny and its evolutionary implications *Annu. Rev. Ecol. Syst.* **45** 371–95
- [3] King N and Rokas A 2017 Embracing uncertainty in reconstructing early animal evolution *Curr. Biol.* **27** R1081–8
- [4] Kramp P L 1961 Synopsis of the medusae of the world *J. Mar. Biol. Assoc. UK* **40** 7–382
- [5] Behrends G and Schneider G 1995 Impact of *Aurelia aurita* medusae (Cnidaria, Scyphozoa) on the standing stock and community composition of mesozooplankton in the Kiel Bight (western Baltic Sea) *Mar. Ecol. Prog. Ser.* **127** 39–45
- [6] Costello J H, Colin S P and Dabiri J O 2008 Medusan morphospace: phylogenetic constraints, biomechanical solutions, and ecological consequences *Invertebrate Biol.* **127** 265–90

- [7] Brusca R C and Brusca G J 2002 *Invertebrates* (Sinauer Associates Incorporated)
- [8] Holstein T W 2022 *The Role of Cnidarian Developmental Biology in Unraveling Axis Formation and Wnt Signaling* (Developmental Biology)
- [9] Gemmell B J, Costello J H, Colin S P, Stewart C J, Dabiri J O, Tafti D and Priya S 2013 Passive energy recapture in jellyfish contributes to propulsive advantage over other metazoans *Proc. Natl Acad. Sci.* **110** 17904–9
- [10] Gemmell B J et al 2015 Suction-based propulsion as a basis for efficient animal swimming *Nat. Commun.* **6** 8790
- [11] Villanueva A, Smith C and Priya S 2011 A biomimetic robotic jellyfish (Robojelly) actuated by shape memory alloy composite actuators *Bioinspir. Biomim.* **6** 036004
- [12] Ren Z, Hu W, Dong X and Sitti M 2019 Multi-functional soft-bodied jellyfish-like swimming *Nat. Commun.* **10** 2703
- [13] Wang T, Joo H-J, Song S, Hu W, Keplinger C and Sitti M 2023 A versatile jellyfish-like robotic platform for effective underwater propulsion and manipulation *Sci. Adv.* **9** eadg0292
- [14] Gemmell B J, Troolin D R, Costello J H, Colin S P and Satterlie R A 2015 Control of vortex rings for manoeuvrability *J. R. Soc. Interface* **12** 20150389
- [15] Dabiri J O, Colin S P, Gemmell B J, Lucas K N, Leftwich M C and Costello J H 2020 Jellyfish and fish solve the challenges of turning dynamics similarly to achieve high maneuverability *Fluids* **5** 106
- [16] Hoover A P, Xu N W, Gemmell B J, Colin S P, Costello J H, Dabiri J O and Miller L A 2021 Neuromechanical wave resonance in jellyfish swimming *Proc. Natl Acad. Sci.* **118** e2020025118
- [17] Pallasdies F, Goedeke S, Braun W and Memmesheimer R-M 2019 From single neurons to behavior in the jellyfish *Aurelia aurita* *elife* **8** e50084
- [18] Costello J, Klos E and Ford M 1998 In situ time budgets of the scyphomedusae *Aurelia aurita*, *Cyanea* sp., and *Chrysaora quinquecirrha* *J. Plankton Res.* **20** 383–91
- [19] McHenry M J and Jed J 2003 The ontogenetic scaling of hydrodynamics and swimming performance in jellyfish (*Aurelia aurita*) *J. Exp. Biol.* **206** 4125–37
- [20] Rueden C T, Schindelin J, Hiner M C, DeZonia B E, Walter A E, Arena E T and Eliceiri K W 2017 ImageJ2: ImageJ for the next generation of scientific image data *BMC Bioinf.* **18** 1–26
- [21] Colin S P, Costello J H, Hansson L J, Titelman J and Dabiri J O 2010 Stealth predation: the ecological success of the invasive ctenophore *Mnemiopsis leidyi* *Proc. Natl. Acad. Sci. USA* **107** 17223–7
- [22] Costello J H, Colin S P, Dabiri J O, Gemmell B J, Lucas K N and Sutherland K R 2021 The hydrodynamics of jellyfish swimming *Annu. Rev. Mar. Sci.* **13** 375–96
- [23] Matharu P S, Wang Z, Costello J H, Colin S P, Baughman R H and Tadesse Y T 2023 SoJel—a 3D printed jellyfish-like robot using soft materials for underwater applications *Ocean. Eng.* **279** 114427
- [24] Frame J, Lopez N, Curet O and Engeberg E D 2018 Thrust force characterization of free-swimming soft robotic jellyfish *Bioinspir. Biomim.* **13** 064001
- [25] Colin S P, Costello J H, Katija K, Seymour J and Kiefer K 2013 Propulsion in cubomedusae: mechanisms and utility *PLoS One* **8** e56393
- [26] Mills S J, Ford J J and Mejias L 2011 Vision based control for fixed wing UAVs inspecting locally linear infrastructure using skid-to-turn maneuvers *J. Intell. Robot. Syst.* **61** 29–42
- [27] Sreenatha A, Rajhans V and Bhardwaj N 1999 Robust controller design for a skid to turn missile *Acta Astronaut.* **45** 85–92
- [28] Stansbery D and Cloutier J 2001 Nonlinear, hybrid bank-to-turn/skid-to-turn missile autopilot design *AIAA Guidance, Navigation, and Control Conf. and Exhibit*
- [29] Fannjiang C, Mooney T A, Cones S, Mann D, Shorter K A and Katija K 2019 Augmenting biologging with supervised machine learning to study in situ behavior of the medusa *Chrysaora fuscescens* *J. Exp. Biol.* **222** jeb207654
- [30] Albert D J 2014 Field observations of four *Aurelia labiata* jellyfish behaviours: swimming down in response to low salinity pre-empted swimming up in response to touch, but animal and plant materials were captured equally *Hydrobiologia* **736** 61–72
- [31] Hamner W, Hamner P and Strand S 1994 Sun-compass migration by *Aurelia aurita* (Scyphozoa): population retention and reproduction in Saanich Inlet *British Columbia. Mar. Biol.* **119** 347–56
- [32] Churnside J H, Marchbanks R D, Donaghay P L, Sullivan J M, Graham W M and Wells R J D 2016 Hollow aggregations of moon jellyfish (*Aurelia* spp.) *J. Plankton Res.* **38** 122–30
- [33] Hamner W M 1995 Sensory ecology of scyphomedusae *Mar. Freshwater Behav. Phys.* **26** 101–18
- [34] Satterlie R 2018 *Jellyfish locomotion Oxford Research Encyclopedia of Neuroscience*
- [35] Katsuki T and Greenspan R J 2013 Jellyfish nervous systems *Curr. Biol.* **23** R592–4
- [36] Satterlie R A 2011 Do jellyfish have central nervous systems? *J. Exp. Biol.* **214** 1215–23
- [37] Horridge G A 1954 The nerves and muscles of medusae. I. Conduction in the nervous system of *Aurelia aurita* Lamarck
- [38] Passano L 1965 Pacemakers and activity patterns in medusae: homage to Romanes *Am. Zool.* **5** 465–81
- [39] Horridge G A 1956 The nerves and muscles of medusae: V. Double innervation in scyphozoa *J. Exp. Biol.* **33** 366–83
- [40] Horridge G A 1959 The nerves and muscles of medusae: VI. The rhythm *J. Exp. Biol.* **36** 72–91
- [41] Hoover A P, Porras A J and Miller L A 2019 Pump or coast: the role of resonance and passive energy recapture in medusan swimming performance *J. Fluid Mech.* **863** 1031–61
- [42] Kim S, Pyeon Y, Lee K, Kim P, Oh W and Choi J H 2020 Visualization of rotational swimming patterns in oblate jellyfish *J. Coast. Res.* **36** 289–94
- [43] Albert D J 2007 *Aurelia labiata* medusae (Scyphozoa) in Roscoe Bay avoid tidal dispersion by vertical migration *J. Sea Res.* **57** 281–7
- [44] Rakow K C and Graham W M 2006 Orientation and swimming mechanics by the scyphomedusa *Aurelia* sp. in shear flow *Limnol. Oceanogr.* **51** 1097–106
- [45] Shanks A L and Graham W M 1987 Orientated swimming in the jellyfish *Stomolopus meleagris* L. Agassiz (Scyphozoa: Rhizostomida) *J. Exp. Mar. Biol. Ecol.* **108** 159–69
- [46] Fossette S, Gleiss A, Chalumeau J, Bastian T, Armstrong C, Vandenabeele S, Karpytchev M and Hays G 2015 Current-oriented swimming by jellyfish and its role in bloom maintenance *Curr. Biol.* **25** 342–7
- [47] Liao J C 2022 Fish swimming efficiency *Curr. Biol.* **32** R666–71
- [48] Hamner W M, Hamner P P, Strand S W and Gilmer R W 1983 Behavior of Antarctic krill, *Euphausia superba*: chemoreception, feeding, schooling, and molting *Science* **220** 433–5